ACS NANO
www.acsnano.org

ARTICLE

Area-Selective Atomic Layer Deposition of Metal Oxides on DNA Nanostructures and Its Applications

Liwei Hui, Rachel Nixon, Nathan Tolman, Jason Mukai, Ruobing Bai, Risheng Wang, and Haitao Liu*

Cite This: *ACS Nano* 2020, 14, 13047−13055 Read Online

ABSTRACT: **We demonstrate area-selective atomic layer deposition (ALD) of oxides on DNA nanostructures. Area-selective ALD of Al_2O_3, TiO_2, and HfO_2 was successfully achieved on both 2D and 3D DNA nanostructures deposited on a polystyrene (PS) substrate. The resulting DNA−inorganic hybrid structure was used as a hard mask to achieve deep etching of a Si wafer for antireflection applications. ALD is a widely used process in coating and thin film deposition; our work points to a way to pattern oxide materials using DNA templates and to enhance the chemical/physical stability of DNA nanostructures for applications in surface engineering.**

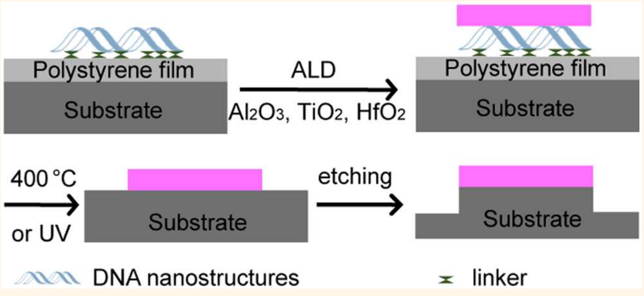

KEYWORDS: *lithography, pattern, antireflection, surface engineering, DNA*

Atomic layer deposition (ALD) is one of the most extensively used tools for surface coating and thin film deposition. It offers precise control over the thickness and composition of the coating and is compatible with a wide range of substrates, flat or curved. Area-selective ALD exploits reactivity differences in the substrate to selectively deposit materials on active sites to produce patterned oxides,[1] nitrides,[2] and metals.[3] Patterning metal oxide on surfaces is important in many fields including integrated circuits,[4] surface engineering,[5,6] and catalysis.[7] Many of these applications require high resolution, designer pattern, and good compatibility with substrates including polymers and other ordinary materials.

The current approaches to realizing area-selective ALD include surface passivation by self-assembled molecular[8−10] or polymer coatings,[11,12] surface activation by UV or e-beam lithography,[13,14] or specific precursor−substrate interactions.[15] Lithography techniques, such as photolithography,[16] laser nanopatterning,[17] and imprinting,[18] are generally used to produce the desired surface patterns. However, the development and applications of these approaches rely highly on advanced instruments. They also often have limitations on the types of substrates in regards to substrate surface flatness and size. Here, we show that DNA nanostructures can mediate area-selective growth of metal oxide on an ALD-inactive surface, producing nanoscale metal oxide patterns that are defined by DNA templates.

DNA nanostructures can be programmed to form virtually any arbitrary shape, irrespective of dimensional complexity and symmetry,[19] simply by changing the DNA strand sequences and assembly conditions.[20] Their sizes are controllable in a tens of nanometers to micrometers range.[21] These structures have been used in electronic circuit design,[22,23] biosensing, and surface engineering applications.[24]

In addition to their tunable structure, DNA nanostructures are chemically functional. Previous work exploited the hydrophilic nature of DNA nanostructures to mediate the water adsorption on a SiO_2 surface, allowing area-selective hydrofluoric acid vapor etching[25] and chemical vapor deposition (CVD) of SiO_2 and TiO_2.[26] Although these reactions are mostly limited to DNA nanostructures deposited on SiO_2 substrate, they did showcase the potential of using DNA nanostructures to achieve a wider range of area-selective surface reactions.

Compared to CVD, ALD offers much better control of the morphology and chemical composition of the coatings. Due to its hydrophilic nature, DNA should promote the nucleation

Received: May 29, 2020
Accepted: September 30, 2020
Published: October 13, 2020

https://dx.doi.org/10.1021/acsnano.0c04493
ACS Nano 2020, 14, 13047−13055

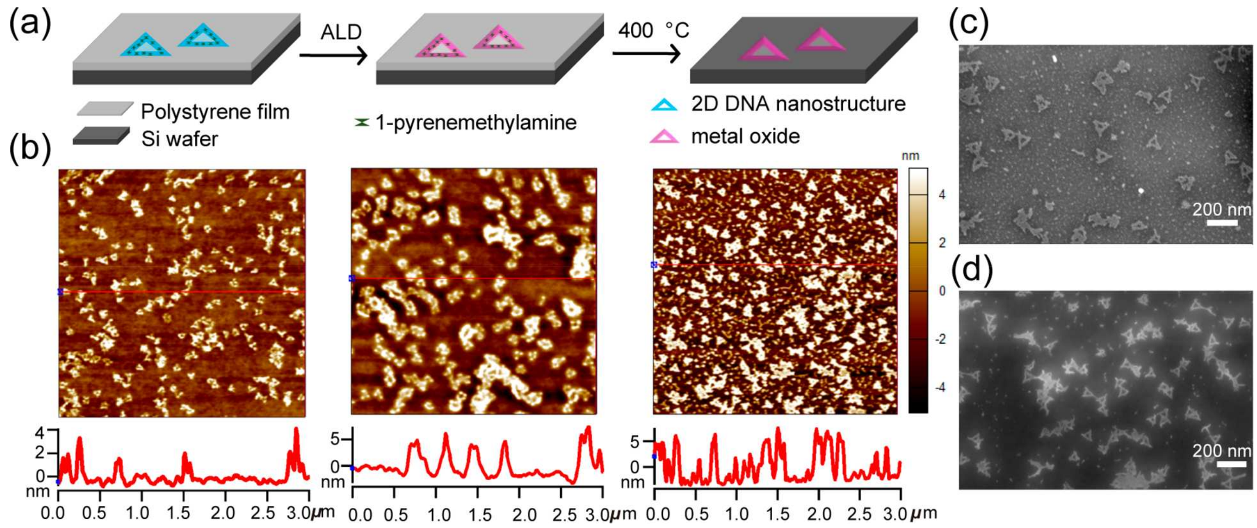

Figure 1. Deposition of 2D DNA nanostructures on PS film and area-selective ALD of metal oxides on the DNA nanostructures. (a) Cartoon illustration of the fabrication steps: deposition of DNA nanostructures on PMA-pretreated PS surface, ALD of metal oxide on the DNA template, and removal of organic compounds to obtain DNA-patterned metal oxide. (b) AFM images and height profiles corresponding to the fabrication steps in the cartoon: (left) DNA triangle deposition on PMA-pretreated PS surface, (middle) Al_2O_3 grown by ALD on DNA-deposited PS surface, and (right) triangle-shaped Al_2O_3 structures obtained after removing the organic support. (c) SEM image of the DNA-patterned Al_2O_3 structures after the organic support was removed by thermal annealing at 400 °C in air for 1 h. (d) SEM image of the DNA-patterned Al_2O_3 structures after removing the organic support. The pulse time for Al_2O_3 ALD precursors was decreased from 0.06 to 0.01 s to increase the selectivity.

and growth of ALD, just as in the case of CVD. To achieve area-selective ALD, an inert substrate will be needed on which to deposit DNA nanostructures. SiO_2 and mica are the two most common substrates for the deposition of DNA nanostructures. However, they are not suitable for area-selective ALD due to their hydrophilic nature, which facilitates nucleation in the background. To make the case even more challenging, ALD precursors are typically much more reactive than those used in CVD, making it especially challenging to suppress background nucleation.

Polymer substrates are particularly attractive for DNA-mediated area-selective ALD. Many polymers are hydrophobic and therefore can inhibit background nucleation during ALD. More significantly, many engineering structures and coatings (*e.g.*, latex paint) are polymer-based. Therefore, developing ways to integrate DNA nanostructures with polymer substrates could have significant scientific and engineering impacts.

There have been no reports in the literature regarding the deposition of DNA nanostructures onto polymers. Most substrates used for depositing DNA nanostructures are hydrophilic and negatively charged (*e.g.*, mica and SiO_2), which interact with DNA *via* a salt bridge structure.[27] DNA nanostructures also adhere to π systems (*e.g.*, highly oriented pyrolytic graphite) *via* hydrophobic and/or $\pi-\pi$ stacking interactions.[28] Inspired by the work of Jin *et al.*,[29] we hypothesized that amphiphilic molecules such as 1-pyrenemethylamine hydrochloride (PMA) could serve as a bridge to anchor DNA nanostructures onto hydrophobic polymer surfaces. The aromatic basal plane of PMA could interact favorably with hydrophobic polymers such as polystyrene (PS), while its amine group with a positive charge could attract DNA nanostructures *via* electrostatic interactions. After DNA nanostructures are deposited, PMA molecules not covered by DNA nanostructures could be removed by solvent washing.

In this study, we developed protocols to deposit DNA nanostructures onto PS substrates, which do not contain any ALD active functional groups.[12] We show that area-selective ALD can be achieved on DNA nanostructures deposited on polystyrene to create patterned metal oxide nanostructures. Such oxide nanostructures can be used as a hard mask for further patterning applications (Figure 1a). As an example, we used the DNA–metal oxide hybrid pattern for deep etching of silicon (Si) for antireflection applications.

RESULTS AND DISCUSSION

Deposition of DNA on Polystyrene. Rothemund's single-layer DNA triangles[30] were employed as a model for 2D DNA nanostructures. This triangle has an outer edge of 122 nm in length and inner hollow edge of 51 nm in length. A thin PS film of ~16 nm in thickness was first spin-coated on a Si wafer, followed by a coating with PMA. Subsequently, DNA triangles were deposited on the PMA-coated PS surface. As expected, on the PMA-pretreated PS surface, DNA nanostructures were well-adhered without any distortion of the shape (Figure 1b); in contrast, on the PS surface without the pretreatment of PMA molecules, a few DNA triangles were adsorbed and they are significantly deformed (Figure S1). This result shows that PMA promotes the adhesion of DNA nanostructures on polystyrene without altering their morphology.

Area-Selective ALD. A standard ALD recipe using trimethylaluminum (TMA) and water as precursors was used to grow Al_2O_3. Atomic force microscopy (AFM) was used to measure the height of DNA triangles on the PS surface. As shown in Figure 1b, the height of DNA triangles was 2.7 ± 0.7 nm on the PS surface. After 50 cycles of growth at 150 °C, it increased to 7.3 ± 0.6 nm. This change is close to the expected ALD growth thickness of 5 nm. This result indicated that the DNA nanostructures selectively initiated growth of Al_2O_3. To get further confirmation that the increase in the height was indeed due to the growth of Al_2O_3, we removed all organic materials by heating the sample at 400 °C in air for 1 h. As

https://dx.doi.org/10.1021/acsnano.0c04493
ACS Nano 2020, 14, 13047−13055

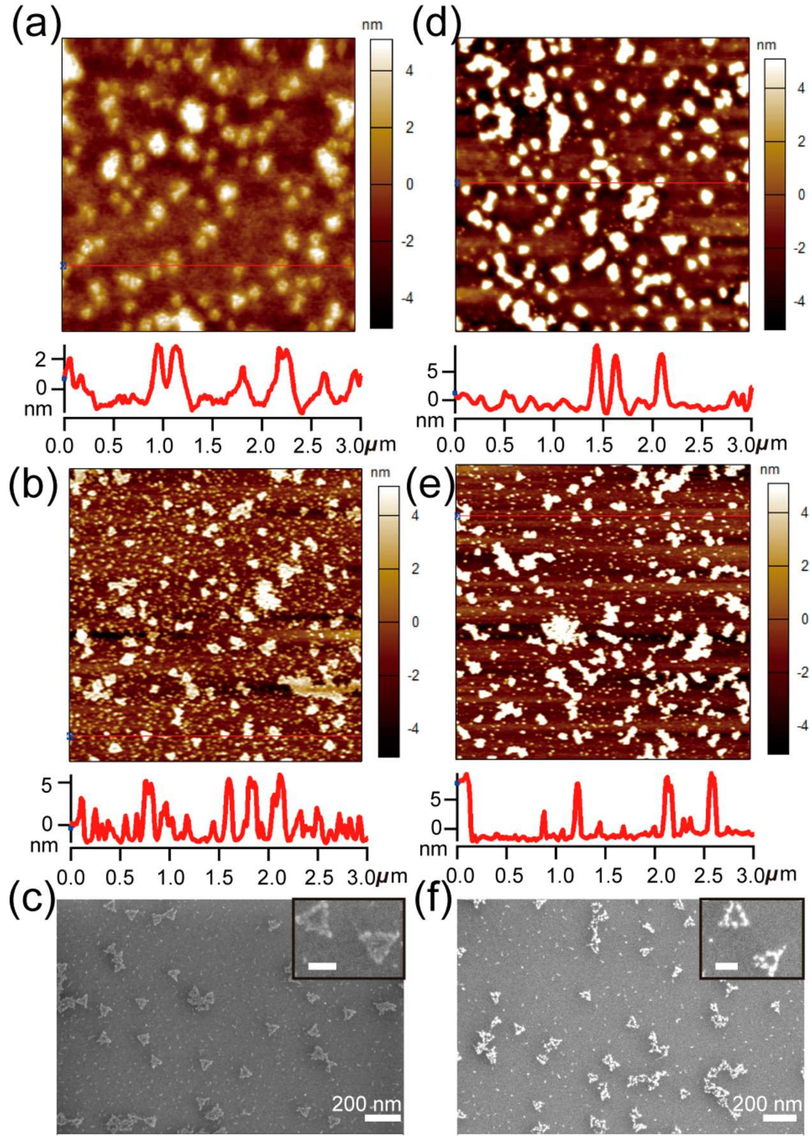

Figure 2. DNA-patterned TiO_2 (a−c) and HfO_2 (d−f) on the PS surface. AFM images and height profiles of (a) TiO_2 growth on the PS surface and (b) TiO_2 patterns preserved after being heated at 400 °C in air. (c) SEM image of TiO_2 patterns after being heated at 400 °C in air. AFM images and height profiles of (d) HfO_2 growth on the PS surface and (e) HfO_2 patterns preserved after being heated at 400 °C in air. (f) SEM images of HfO_2 patterns after being heated at 400 °C in air. Insets in (c) and (f) show magnified views of the samples; scale bars in the insets are 50 nm.

shown in Figure 1b, the height of the triangle shapes after being heated was 9.0 ± 0.7 nm, similar to the heights measured before being heated. Scanning electron microscopy (SEM) images of the heat-treated ALD samples also showed hollow triangle patterns (Figure 1c). Although thermal annealing may result in Ostwald ripening of metal oxide nanoparticles,[31] it did not influence the Al_2O_3 pattern we obtained here. As an alternative to thermal annealing, we used UV/ozone treatment (4 h) to remove the organic materials. As shown in Figure S2, the surface of the UV/ozone treatment showed triangle morphology, which was similar to that of the annealed sample. It is worth noting that the edge length of the Al_2O_3 triangle before being thermally annealed (162.6 ± 15.3 nm) was larger than that of the DNA template (139.9 ± 9.9 nm). Although an increase of edge length is expected due to the conformal nature of ALD, the increase is larger than expected. In addition, edge length decreased after being thermally annealed (143.6 ± 15.1 nm). We speculate that the PS has high fluidity at the ALD temperature, and the PS film reflows to wet the newly formed Al_2O_3 structure, making the structures appear larger under AFM than they really are (*vide infra*).

Using an appropriate concentration of PMA linker was critical to both the morphological integrity of the DNA templates and the selectivity of ALD growth. As shown in Figure S3a,b, increasing the PMA concentration increased the roughness of the PS surface after the ALD. Tiny, randomly distributed nanoparticles were observed after ALD, which were attributed to the nucleation induced by PMA residuals on the PS surface. We also observed evidence of ALD infiltration,[32] which is the nucleation and growth of oxides inside/underneath the PS film. As can be seen in Figure 1b, small particles appeared after the PS film was removed; we believe that these particles are Al_2O_3 formed due to ALD infiltration (also see Figure S3c). The infiltration of ALD precursors depends on the porosity of the PS film and the solubility of ALD precursors in the polymer film, as evidenced by ALD

https://dx.doi.org/10.1021/acsnano.0c04493
ACS Nano 2020, 14, 13047−13055

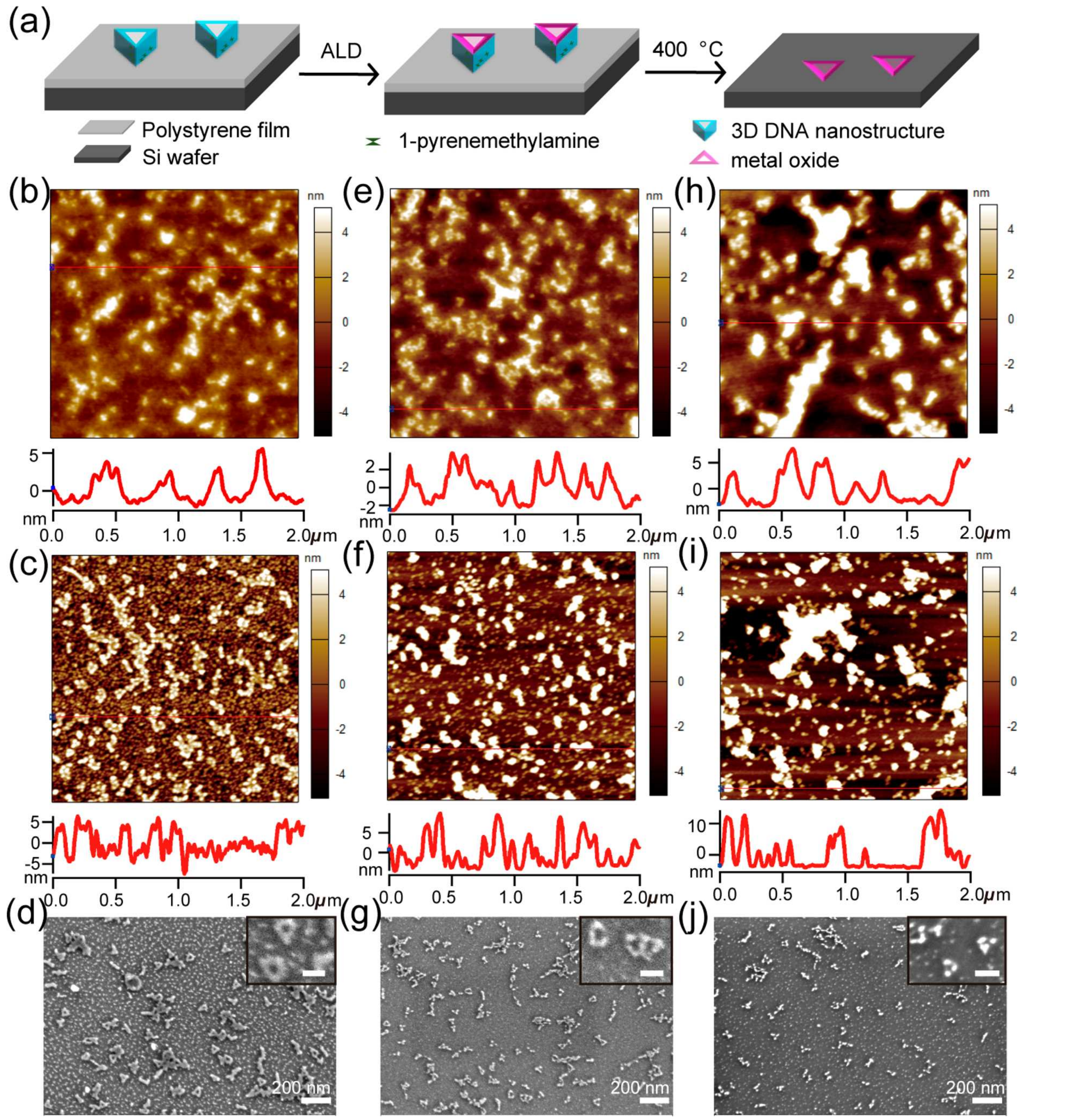

Figure 3. Deposition of 3D DNA nanostructures on PS film and area-selective ALD of metal oxides on the 3D DNA nanostructures. (a) Cartoon illustration of the fabrication steps: deposition of 3D DNA nanostructures on PMA-pretreated PS surface, ALD of metal oxide on the 3D DNA templates, and removal of organic supports to obtain DNA-patterned metal oxide. (b−j) 3D DNA triangle-templated (b−d) Al_2O_3, (e−g) TiO_2, and (h−j) HfO_2 on PS surface. AFM images and height profiles of (b,e,h) metal oxide deposited on PS surface and (c,f,i) metal oxide patterns after being heated in air at 400 °C. (d,g,j) SEM images of metal oxide patterns after being heated in air at 400 °C. Insets in (d,g,j) show magnified views of the nanostructures; scale bars in the insets are 50 nm.

results with different polymer film thickness (Figure S4), ALD temperature (Figure S5a,d), and number of ALD cycles (Figure S5e,f). The optimized ALD execution temperature was 150 °C, which is higher than the glass transition temperature T_g of such thin PS films (~86 °C).[33] Due to the porosity of the PS film and ALD precursors trapped in the PS film, ALD execution at low temperature would lead to uniform nucleation and thus the loss of selectivity (Figure S5a,b). Increasing the temperature would promote the desorption of ALD precursors in the film but at the expense of increasing nucleation and growth rate, which will eventually reduce the selectivity (Figure S5c,d). A more straightforward approach to increase ALD selectivity is to decrease the soluble amount of ALD precursors in the PS film. As shown in Figures 1d and S6, by decreasing the pulse time of both TMA and H_2O precursors from 0.06 to 0.01 s, undesired aggregates in the background were significantly eliminated, while the Al_2O_3 growth on the DNA template remained the same (8.9 ± 0.5 nm).

We used the same approach to carry out area-selective ALD of TiO_2 and HfO_2, using tetrakis(dimethylamido)titanium (TDMAT) and tetrakis(dimethylamido)hafnium (TDMAH) as precursors, respectively. We found that the ALD infiltration

https://dx.doi.org/10.1021/acsnano.0c04493
ACS Nano 2020, 14, 13047−13055

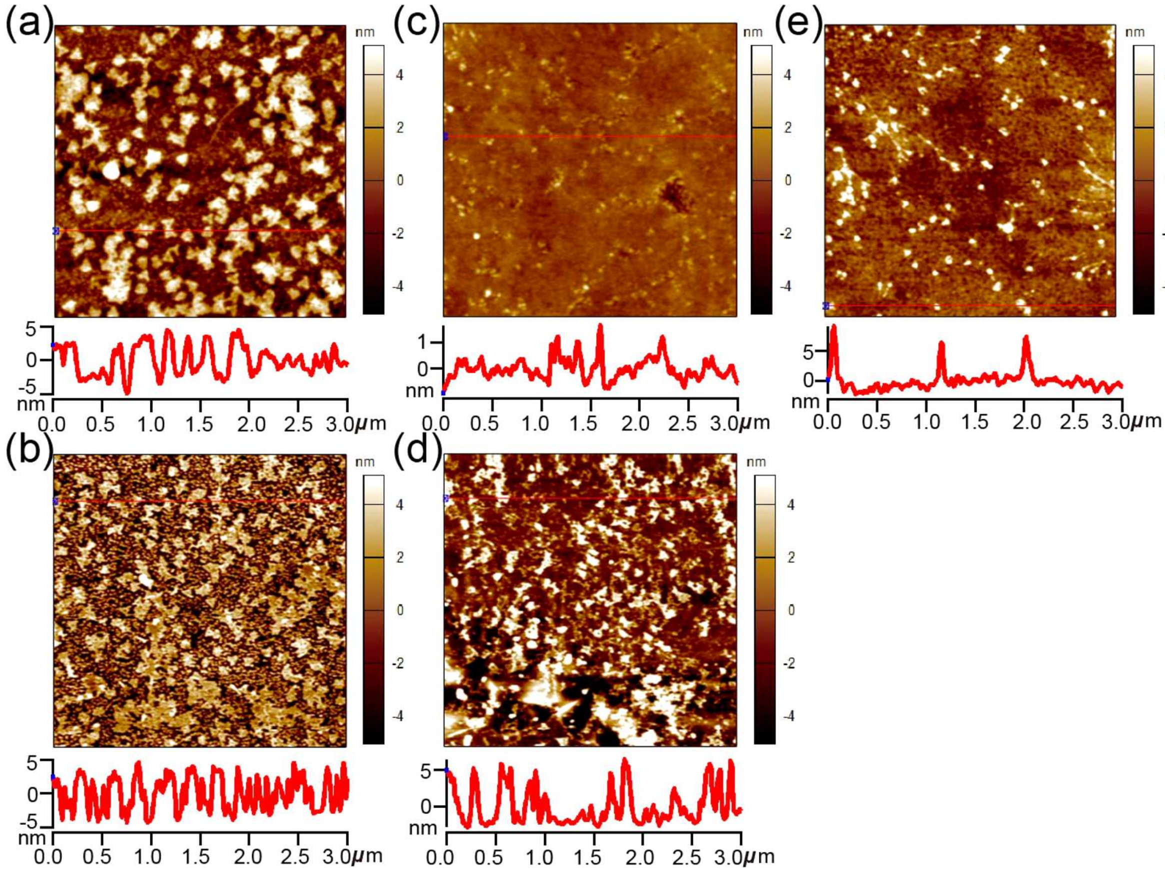

Figure 4. AFM images and height profiles of 2D DNA triangle-patterned Al_2O_3 on PS surface fabricated on different substrates including (a,b) quartz, (c,d) glass slides, and (e) PDMS. (a,c,e) Al_2O_3 growth on PS surface and (b,d) Al_2O_3 patterns preserved after being heated in air at 400 °C.

is much less pronounced for these two precursors (Figure S7).[34] As an example, we ran 100 cycles of TiO_2 deposition and 50 cycles of HfO_2 deposition, which ideally should produce 4.7 nm of TiO_2 deposition and 5.8 nm of HfO_2 deposition, respectively. As shown in Figure 2a,b, the height of triangular TiO_2 patterns was 4.3 ± 0.9 nm after 100 ALD cycles and increased to 7.1 ± 0.5 nm after the removal of organic materials by being heated in air. Note that the measured height of DNA-patterned TiO_2 increased after the removal of organics, similar to the case of Al_2O_3. We attribute this observation to the fluidity of PS at the ALD temperature ($T > T_g$) and the change of the AFM tip−sample interaction in the background (*i.e.*, from soft PS surface to the hard Si surface) (Figure S8).[35] When the PS surface was incubated in the same ALD chamber but without precursor pulses, the roughness of the bare PS surface changed from 177.4 ± 9.6 to 243.0 ± 15.8 pm (Figure S9a,b). Meanwhile, the edge length of the DNA triangle shrunk slightly, suggesting high fluidity of PS chains around DNA nanostructures (Figure S9c,d). Similarly, the thickness of the triangular HfO_2 pattern was 9.9 ± 0.6 nm after the 50 cycles of ALD deposition; the height increased to 10.3 ± 0.4 nm after the removal of organics by being heated in air (Figure 2d,e).

Both TiO_2 and HfO_2 nanostructures survived the thermal annealing treatment at 400 °C (Figure 2c,f), although signs of Ostwald ripening can be seen on both types of structures.[36] The edges of the TiO_2 triangle structure were rough; the HfO_2 structures broke into triangle frames of tiny nanoparticles. This change of morphology may reflect the precursor attachment, nucleation, and coalescence of oxide particles during ALD. For both TDMAH and TDMAT precursors, the relatively low reactivity and high mobility lead to initial incomplete deposition, which reorganizes to form such nonconformal frame structures.[37]

Additional experiments showed that the PS substrate inhibited ALD nucleation for up to 150 cycles. In one set of experiments, we found that the height of TiO_2 triangle patterns was 1.8 ± 0.5 nm for 50 cycles and 6.7 ± 0.5 nm for 150 cycles, both measured before the removal of organics. After the removal of organics, the height of the triangle patterns increased to 4.2 ± 0.4 nm for 50 cycles and 9.7 ± 1.5 nm for 150 cycles (Figure S10); these values are consistent with the expected ALD deposition thicknesses of 2.4 and 7.1 nm, respectively, suggesting area selectivity up to 150 cycles.

We found that ALD infiltration is greatly reduced for both TiO_2 and HfO_2 when compared to that of Al_2O_3. In the case of Al_2O_3 ALD, the DNA-templated Al_2O_3 pattern was not observed when a thicker (*e.g.*, >31 nm *versus* 16 nm) PS film was used (Figure S4), which we attributed to the increased trapping of ALD precursors in the thicker film. However, in the cases of TiO_2 and HfO_2, the morphology of the DNA-templated triangle pattern was well-preserved on thicker PS films. As shown in Figure S11, after ∼5 nm of ALD growth of TiO_2 and HfO_2 on ∼157 nm thick PS film, the triangle patterns were clearly observed after the organics were removed. Note that, in this case, the PS surface was rough, making the imaging of oxide patterns difficult before the removal of organics (Figure S11a,d). The heights of the triangle patterns

https://dx.doi.org/10.1021/acsnano.0c04493
ACS Nano 2020, 14, 13047−13055

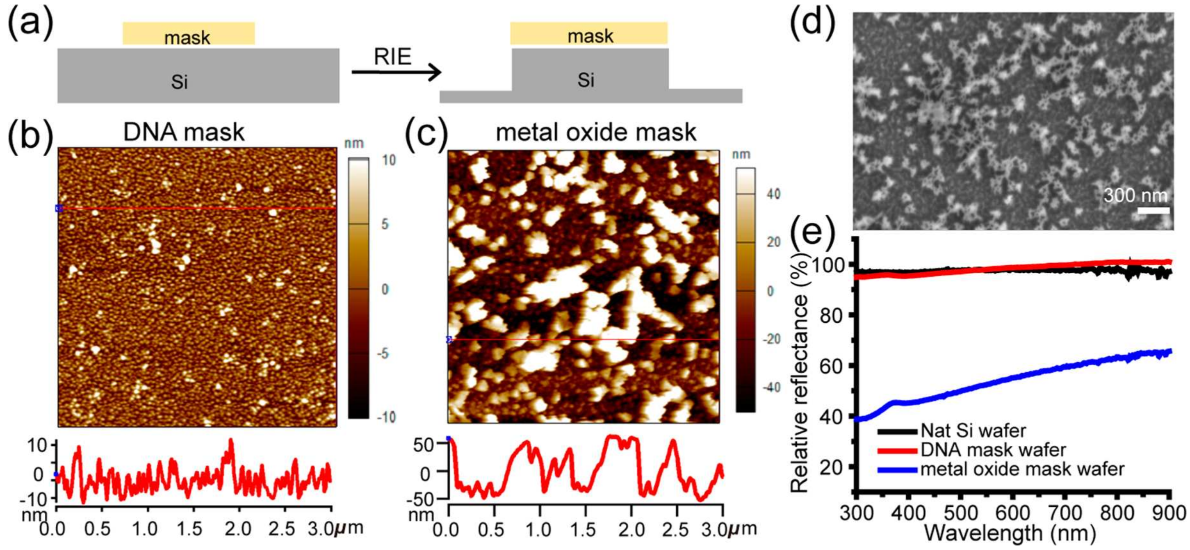

Figure 5. DNA-mediated etching of Si. (a) Schematics of RIE of the Si wafer. AFM images and height profiles of the etched wafer using (b) unmodified DNA nanostructures as a mask and (c) DNA−metal oxide hybrid nanostructures as masks. (d) SEM images of the Si wafer patterned using the DNA−metal oxide hybrid nanostructures. (e) Antireflection property of the Si wafer surface measured with a microspectrophotometer, including native oxide Si wafer (black), DNA-templated etched Si wafer (red), and DNA−metal oxide hybrid-templated etched Si wafer (blue). A piece of bare Si wafer surface was used as reference with a reflectance of 100% across the wavelength of 300−900 nm to calibrate the setup. Each line was reported as the average of reflection spectra on the center of two different samples.

were 9.7 ± 2.6 and 11.4 ± 1.2 nm for TiO_2 and HfO_2 patterns, respectively. Together, these results showed consistent area-selective ALD of metal oxides on DNA templates.

Extension to 3D DNA Templates. To test the feasibility of 3D ALD coating, we used a 3D DNA triangle as a model (Figure 3a). This nanostructure was assembled by using 14-helix bundle packed into a honeycomb lattice on each edge.[38] The edge of the 3D DNA triangles was ∼50 nm long, and the cross section of the edge was about 6 nm × 12 nm (width × height). Once dried in air, the height of 3D DNA triangle decreased to ∼4 nm due to shrinkage (Figure S12a). Similar to the case of 2D DNA nanostructures, the 3D DNA triangles could also be deposited onto the PS surface with the help of PMA linkers (Figure S12b). After ALD of Al_2O_3, TiO_2, and HfO_2 was performed (Figure 3b,e,h, respectively) and the organics removed (Figure 3c,f,i), the heights of the triangle patterns were 7.2 ± 0.7, 9.4 ± 1.7, and 10.5 ± 1.0 nm, respectively. Due to the smaller lateral size of the 3D DNA template, the AFM images did not clearly show the morphology. However, as can be seen in the SEM images (Figure 3d,g,j), all three types of oxide patterns indeed maintained their hollow triangle shapes. Interestingly, we found that the height of deposited metal oxide on the 3D DNA template was similar to that on the 2D DNA template, suggesting the ALD was largely localized to the top surface of the DNA templates. We speculate that this phenomenon may be linked to the high mobility of PS molecules at the ALD temperature, which allows it to shield the sides of the 3D DNA nanostructure. Overall, our results showed excellent area selectivity in the ALD growth.

Extension to Other Substrates. Our approach to area-selective ALD can be applied to any substrate that can be coated with a thin layer of PS film. As examples, we showed that the 2D triangle-patterned Al_2O_3 can be prepared on quartz, common glass slides, and polydimethylsiloxane (PDMS) substrates. As shown in Figure 4, in all cases, Al_2O_3 triangle nanostructures were obtained from the 2D DNA triangle nanostructure template, and their morphologies highly resembled that of the templates.

Applications in Lithography. The metal oxide nanostructures can serve as hard masks to produce high-aspect-ratio patterns on the underlying substrate. DNA-based nanofabrication has undergone extensive advances in recent years. High-resolution patterning has been achieved using DNA nanostructures as the template.[24] However, the etching depth and aspect ratio of the transferred patterns are still limited due to limited chemical stability of DNA nanostructure. .

The metal oxide nanostructures we prepared here should be compatible with the harsh etching conditions used in many plasma-based deep etching processes. To explore this possibility, we used the Al_2O_3 structure templated by a 2D DNA triangle as a hard mask for SF_6/O_2 reactive ion etching (RIE) of a Si wafer (Figure 5a). As a control, we used the 2D DNA triangle itself as a mask for the RIE and found that the etched pattern was less than 20 nm (Figure 5b) in height. In contrast, when using a DNA−metal oxide hybrid nanostructure as a mask in RIE, the etched patterns were 106.2 ± 17.8 nm (Figure 5c) in height. More importantly, as shown by SEM, the patterns fabricated using a DNA−metal oxide hybrid showed both the triangular shape and the inner hollow cavity, both prominent features of the DNA template (Figure 5d). The aspect ratio of the patterns prepared using DNA−metal oxide hybrid nanostructures is greater than 5, whereas that of the patterns prepared using DNA nanostructures is less than 1. This result highlights the advantage of using DNA-templated metal oxides as a hard mask for deep etching.

Such high-aspect-ratio nanoscale patterns can significantly reduce surface reflection as suggested by our finite-difference time-domain (FDTD) simulation (Figure S13). We used a microspectrophotometer to measure the reflectance spectrum of Si wafers in the range of 300−900 nm. Using a bare Si wafer as the reference (*i.e.*, 100% reflectance), we found the reflectance was reduced by 40−60% once the Si wafer was patterned with DNA−oxide hybrid structures. In contrast, the

https://dx.doi.org/10.1021/acsnano.0c04493
ACS Nano 2020, 14, 13047−13055

Si wafer templated by DNA nanostructures (not coated by ALD) still showed close to 100% reflectance (Figure 5e). In another control, we replaced the DNA dispersion with a buffer solution and kept all other processing steps the same. In this case, small Al_2O_3 particles were produced by ALD infiltration. However, these small particles did not produce any high-aspect-ratio pattern after the plasma etching, and the reflectance was reduced by approximately <5% (Figure S14).

The antireflection property highly depends on the density of the nanostructured pillars. We found that the relative reflectance at 400 nm was higher (68%) in the center than at the edge (16%). This difference in the reflectance was due to the difference in the density of DNA triangle templates, which was 28% in the center *versus* 79% at the edge (Figure S15). This gradient distribution of DNA nanostructures is due to the "coffee ring effects"; that is, when the DNA nanostructures were deposited onto the PS film, the density of DNA nanostructures was higher at the edge of the droplet than in the center.[39] For future applications, it will be important to achieve controlled, homogeneous deposition of DNA nanostructures on solid substrates.

CONCLUSIONS

In summary, we have developed an area-selective ALD of Al_2O_3, TiO_2, and HfO_2 on both 2D and 3D DNA nanostructures. The DNA-patterned metal oxide hybrid could be prepared on a variety of substrates using a PS film as an intermediate layer. The DNA−metal oxide hybrid nanostructure significantly improved the chemical stability of DNA, allowing it to be used as a hard mask for deep etching of Si using RIE. The etched wafers showed significant reduction of reflection in the visible spectrum. This work allows DNA nanostructures to be used for patterning polymers and many other types of substrates using conventional gas-phase etching processes.

METHODS

Materials. Native oxide silicon wafer (p-doped, ⟨100⟩) was purchased from University Wafer. Short DNA staple strands were ordered from IDT Technology. M13mp18 single-strand phage DNA was purchased from Bayou Biolabs. Polystyrene (M_w = 280,000) and 1-pyrenemethylamine hydrochloride (95%), toluene (99.5%) and magnesium acetate tetrahydrate (99%) were purchased from Sigma-Aldrich. TAE buffer was purchased from Thermo Scientific. Ethanol (Ethanol 200, anhydrous) was ordered from Decon Laboratories Inc. Uranyl acetate (98%) was ordered from VMR. PDMS was prepared by following the recipe of the Sylgard 184 silicone elastomer kit (Dow Corning). The AFM tip (HQ:NSC15/AlBS) was ordered from NanoAndMore.

Preparation of DNA Nanostructure Dispersions. Two-dimensional DNA triangles were prepared *via* a previous report.[30] Briefly, a mixture of M13mp18 strands (8.6 μL, 1 mg/mL), staple strands (15 μL, 300 nM for each staple strand), and 1× TAE/Mg^{2+} (40 mM Tris, 20 mM acetic acid, 1 mM EDTA, and 12.5 mM magnesium acetate) was annealed from 95 to 20 °C at a rate of 1 °C/min. Three-dimensional DNA triangles were also prepared *via* a previous protocol.[38] Similarly, the M13mp18 scaffold and the staple strands were mixed together at molar ratio of 1:5 of 1× TAE/Mg^{2+}, followed by annealing from 90 to 16 °C for over 12 h. Subsequently, both 2D- and 3D-annealed mixtures were filtered through an ultrafiltration tube (Pall Co., Nanosep, MWCO: 30 kDa) and washed with 1× TAE/Mg^{2+} to remove the free staples and to purify the structures. After three rounds of filtration, the received DNA nanostructures were diluted using 1× TAE/Mg^{2+} to a concentration of ∼3 μg/mL for further use.

DNA-Patterned ALD Growth. First, PS stock solutions in toluene were spin-coated on different substrates at 3000 rpm for 30 s. The optimized concentration of PS stock solution was 4 mg/mL for the native oxide Si wafer and quartz, 30 mg/mL for glass slides, and 20 mg/mL for PDMS. Second, the PS-coated substrate was covered with PMA solution (0.5 mg/mL in methanol) for 5 min. Following that, the PMA solution was quickly blown away with nitrogen flow. The obtained surface was subsequently covered with DNA triangle dispersions and incubated for another 10 min. DNA triangle dispersions were removed by nitrogen, and the obtained surface was gently washed once with an ethanol/H_2O mixture (ethanol/H_2O (v/v) = 9:1). Third, a standard thermal ALD recipe at 150 °C provided by Veeco was executed using an Ultratech/Cambridge Fiji G2 Plasma-Enhanced ALD instrument. For Al_2O_3 ALD, trimethylaluminum and H_2O were used as precursors. The pulse time for TMA and H_2O were both 0.06 s, whereas the pulse duration was 10 s for both. For the recipe to reduce the injection amount of precursors, the pulse times for TMA and H_2O were both changed to 0.01 s, whereas the other conditions, including pulse duration, were all the same. The recipe was run for 50 cycles, and expected growth per cycle on the Si wafer was 0.99 Å. For TiO_2 ALD, tetrakis(dimethylamido)titanium and H_2O were used as precursors. The pulse time for H_2O and TDMAT was 0.06 and 0.25 s, respectively, and the purge duration for TDMAT and H_2O was 15 s for both. The recipe was run for 100 cycles, and expected growth per cycle on the Si wafer was 0.47 Å. For HfO_2 growth, tetrakis(dimethylamido)hafnium and H_2O were used as precursors. The pulse time for H_2O and TDMAH was 0.06 and 0.25 s, respectively. The purge duration for TDMAH and H_2O was 15 s for both. The recipe was run for 50 cycles, and expected growth per cycle on Si wafer was 1.17 Å.

Atomic Force Microscopy Analysis. The surface morphology and height profiles of the patterns were obtained using an Asylum MFP 3D in AC air tapping mode. All scans were 3 μm × 3 μm. The obtained data were analyzed using Igor Pro and vendor supplied software.

Ellipsometry Measurement. The thickness of each PS film was measured with an Alpha-SE spectroscopic ellipsometer (J.A. Woollam Co.) with an incident angle of 70°. The data were fitted using the software provided by the vendor (CompleteEASE).

Scanning Electron Microscopy Analysis. The morphology of DNA−metal oxide hybrid pattern on the Si wafer was imaged using a ZEISS Sigma500 VP microscope. Before imaging, the organic components of the ALD sample were removed by thermal annealing or UV/ozone.

Etching of Si Wafer. Reactive ion etching was performed using a Trion Technology Orion III reactive ion etching system. The following SF_6/O_2 plasma etching recipe was used: 20 sccm SF_6; 8 sccm O_2; pressure = 25 mTorr; RF power = 100 W. The recipe was run for 4 s. For the control sample of DNA itself as a template, a 2D DNA triangle dispersion was deposited on a native oxide Si wafer and stained with a drop of 1% uranyl acetate for 1 min. Subsequently, the surface was washed with an ethanol/H_2O mixture and etched with the above RIE recipe. For the control sample of the w/o pattern etched Si wafer, the wafer was prepared by coating buffer on the PMA-pretreated PS surface, performing Al_2O_3 ALD, heating at 400 °C in air for 1 h, and etching for 4 s.

Reflectance Spectra Measurements. The reflectance spectra of the Si wafers were measured using a CRAIC QDI 2010 UV−Vis/NIR microspectrophotometer. The power source was a 75 W Xe lamp. A native oxide Si wafer was used as reference (*i.e.*, 100% reflection across the wavelength range from 300 to 900 nm). To investigate the spatial variation of the reflection, the spectrum was collected from the pattern center to edge successively with each measurement, covering a view of 75 μm × 75 μm.

Finite-Difference Time-Domain Simulations. The theoretical reflectance spectra of the Si wafer surface were simulated using Lumerical FDTD solutions. The substrate was Si and coated with a layer of SiO_2 with the thickness of 1 nm (*i.e.*, native oxide). The hollow triangle-shaped nanopillars have the following geometry: height = 100 nm; outer edge length = 120 nm; inner edge length = 50

https://dx.doi.org/10.1021/acsnano.0c04493
ACS Nano 2020, 14, 13047−13055

nm. The distance between the hollow triangle pillars was 300 nm, which is close to the average pattern-to-pattern distance in the center region of the etched wafer. The simulation boundary was periodic for *x* and *y* axes and was a perfectly matched layer for the *z* axis. A plane wave was used as the light source with a wavelength range of 300−900 nm.

ASSOCIATED CONTENT

Supporting Information

The Supporting Information is available free of charge at https://pubs.acs.org/doi/10.1021/acsnano.0c04493.

> Morphology of DNA deposited on PS, DNA deposited on a PMA-pretreated PS surface, DNA-patterned Al_2O_3 structures after the organic support was removed by UV/ozone treatment, DNA-Al_2O_3 nanostructures grown on thicker PS films, DNA−Al_2O_3 nanostructures grown under different ALD condition, DNA−Al_2O_3 nanostructures grown with ALD precursor pulse time of 0.01 s, TiO_2 and HfO_2 ALD infiltration, PS and DNA on PS after 150 °C incubation, DNA−TiO_2 nanostructures with different ALD cycles, DNA−TiO_2 and DNA−HfO_2 grown on thicker PS film, and 3D DNA triangles on Si wafer and PMA-pretreated PS surface; FDTD simulated reflectance spectra; morphology and reflection spectra of Si wafer etched without DNA template; antireflection property as a function of the density of nanoscale patterns (PDF)

AUTHOR INFORMATION

Corresponding Author

Haitao Liu − *Department of Chemistry, University of Pittsburgh, Pittsburgh, Pennsylvania 15260, United States;* orcid.org/0000-0003-3628-5688; Email: hliu@pitt.edu

Authors

Liwei Hui − *Department of Chemistry, University of Pittsburgh, Pittsburgh, Pennsylvania 15260, United States;* orcid.org/0000-0002-7123-3157

Rachel Nixon − *Department of Chemistry, Missouri University of Science and Technology, Rolla, Missouri 65409, United States*

Nathan Tolman − *Department of Chemistry, University of Pittsburgh, Pittsburgh, Pennsylvania 15260, United States*

Jason Mukai − *Department of Chemistry, University of Pittsburgh, Pittsburgh, Pennsylvania 15260, United States*

Ruobing Bai − *Department of Chemistry, University of Pittsburgh, Pittsburgh, Pennsylvania 15260, United States*

Risheng Wang − *Department of Chemistry, Missouri University of Science and Technology, Rolla, Missouri 65409, United States;* orcid.org/0000-0001-6539-1565

Complete contact information is available at: https://pubs.acs.org/10.1021/acsnano.0c04493

Notes

The authors declare no competing financial interest.

ACKNOWLEDGMENTS

H.L. acknowledges financial support from ONR (N000141812555). We gratefully thank Dr. Esta Abelev, Matthew France, Dr. Jun Chen, and Dr. Daniel Lamont from the Nanoscale Fabrication and Characterization Facility at the University of Pittsburgh for their great help with ALD, RIE, and microspectrophotometer instruments. We thank Prof. Lei Li (University of Pittsburgh) for assistance with ellipsometry measurements. This work was supported, in part, by the National Science Foundation Grant No. CCF-1814797 to R.W.

REFERENCES

(1) Stevens, E.; Tomczak, Y.; Chan, B. T.; Altamirano Sanchez, E.; Parsons, G. N.; Delabie, A. Area-Selective Atomic Layer Deposition of TiN, TiO_2, and HfO_2 on Silicon Nitride with Inhibition on Amorphous Carbon. *Chem. Mater.* **2018**, *30*, 3223−3232.

(2) Lecordier, L.; Herregods, S.; Armini, S. Vapor-Deposited Octadecanethiol Masking Layer on Copper to Enable Area Selective Hf_3N_4 Atomic Layer Deposition on Dielectrics Studied by *in Situ* Spectroscopic Ellipsometry. *J. Vac. Sci. Technol., A* **2018**, *36*, 031605.

(3) Zyulkov, I.; Krishtab, M.; De Gendt, S.; Armini, S. Selective Ru ALD as a Catalyst for Sub-Seven-Nanometer Bottom-Up Metal Interconnects. *ACS Appl. Mater. Interfaces* **2017**, *9*, 31031−31041.

(4) Sim, K.; Rao, Z. L.; Zou, Z. N.; Ershad, F.; Lei, J. M.; Thukral, A.; Chen, J.; Huang, Q. A.; Xiao, J. L.; Yu, C. J. Metal Oxide Semiconductor Nanomembrane-Based Soft Unnoticeable Multifunctional Electronics for Wearable Human-Machine Interfaces. *Sci. Adv.* **2019**, *5*, No. eaav9653.

(5) Ghanashyam Krishna, M.; Vinjanampati, M.; Dhar Purkayastha, D. Metal Oxide Thin Films and Nanostructures for Self-Cleaning Applications: Current Status and Future Prospects. *Eur. Phys. J.: Appl. Phys.* **2013**, *62*, 30001.

(6) Liu, H. Y.; Peng, J. J.; Liu, W. M.; Wang, Y. L.; Wu, J. H.; Zhang, G. L.; Wang, X. L.; Yan, Y. Strong Interference-Based Ultrathin Conductive Anti-Reflection Coating on Metal Substrates for Optoelectronics. *NPG Asia Mater.* **2018**, *10*, 309−317.

(7) Zhao, G. F.; Yang, F.; Chen, Z. J.; Liu, Q. F.; Ji, Y. J.; Zhang, Y.; Niu, Z. Q.; Mao, J. J.; Bao, X. H.; Hu, P. J.; Li, Y. D. Metal/Oxide Interfacial Effects on the Selective Oxidation of Primary Alcohols. *Nat. Commun.* **2017**, *8*, 14039.

(8) Chen, R.; Bent, S. F. Chemistry for Positive Pattern Transfer Using Area-Selective Atomic Layer Deposition. *Adv. Mater.* **2006**, *18*, 1086−1090.

(9) Minaye Hashemi, F. S.; Prasittichai, C.; Bent, S. F. Self-Correcting Process for High Quality Patterning by Atomic Layer Deposition. *ACS Nano* **2015**, *9*, 8710−8717.

(10) Liu, X.; Zhu, Q. Q.; Lang, Y.; Cao, K.; Chu, S. Q.; Shan, B.; Chen, R. Oxide-Nanotrap-Anchored Platinum Nanoparticles with High Activity and Sintering Resistance by Area-Selective Atomic Layer Deposition. *Angew. Chem., Int. Ed.* **2017**, *56*, 1648−1652.

(11) Ellinger, C. R.; Nelson, S. F. Selective Area Spatial Atomic Layer Deposition of ZnO, Al_2O_3, and Aluminum-Doped ZnO Using Poly(vinyl Pyrrolidone). *Chem. Mater.* **2014**, *26*, 1514−1522.

(12) Peng, Q.; Tseng, Y. C.; Darling, S. B.; Elam, J. W. Nanoscopic Patterned Materials with Tunable Dimensions *via* Atomic Layer Deposition on Block Copolymers. *Adv. Mater.* **2010**, *22*, 5129−5133.

(13) Huang, J.; Lee, M.; Lucero, A.; Cheng, L. X.; Kim, J. Area-Selective ALD of TiO_2 Nanolines with Electron-Beam Lithography. *J. Phys. Chem. C* **2014**, *118*, 23306−23312.

(14) Mameli, A.; Karasulu, B.; Verheijen, M. A.; Barcones, B.; Macco, B.; Mackus, A. J. M.; Kessels, W. M. M. E.; Roozeboom, F. Area-Selective Atomic Layer Deposition of ZnO by Area Activation Using Electron Beam-Induced Deposition. *Chem. Mater.* **2019**, *31*, 1250−1257.

(15) Mackus, A. J. M.; Verheijen, M. A.; Leick, N.; Bol, A. A.; Kessels, W. M. M. Influence of Oxygen Exposure on the Nucleation of Platinum Atomic Layer Deposition: Consequences for Film Growth, Nanopatterning, and Nanoparticle Synthesis. *Chem. Mater.* **2013**, *25*, 1905−1911.

(16) Guo, L.; Lee, I.; Zaera, F. Patterning of Solid Films *via* Selective Atomic Layer Deposition Based on Silylation and UV/Ozonolysis. *ACS Appl. Mater. Interfaces* **2016**, *8*, 19836−19841.

(17) Wang, B.; Wang, X. C.; Zheng, H. Y.; Lam, Y. C. Surface Modification of Polystyrene by Femtosecond Laser Irradiation. *J. Laser Micro/Nanoeng.* **2016**, *11*, 253−256.

(18) Jiang, X.; Bent, S. F. Area-Selective ALD with Soft Lithographic Methods: Using Self-Assembled Monolayers to Direct Film Deposition. *J. Phys. Chem. C* **2009**, *113*, 17613−17625.
(19) Seeman, N. C. Nucleic-Acid Junctions and Lattices. *J. Theor. Biol.* **1982**, *99*, 237−247.
(20) Wang, P. F.; Meyer, T. A.; Pan, V.; Dutta, P. K.; Ke, Y. G. The Beauty and Utility of DNA Origami. *Chem.* **2017**, *2*, 359−382.
(21) Wang, P. F.; Gaitanaros, S.; Lee, S.; Bathe, M.; Shih, W. M.; Ke, Y. G. Programming Self-Assembly of DNA Origami Honeycomb Two-Dimensional Lattices and Plasmonic Metamaterials. *J. Am. Chem. Soc.* **2016**, *138*, 7733−7740.
(22) Tapio, K.; Leppiniemi, J.; Shen, B. X.; Hytonen, V. P.; Fritzsche, W.; Toppari, J. J. Toward Single Electron Nanoelectronics Using Self-Assembled DNA Structure. *Nano Lett.* **2016**, *16*, 6780−6786.
(23) Gates, E. P.; Dearden, A. M.; Woolley, A. T. DNA-Templated Lithography and Nanofabrication for the Fabrication of Nanoscale Electronic Circuitry. *Crit. Rev. Anal. Chem.* **2014**, *44*, 354−370.
(24) Hui, L. W.; Zhang, Q. M.; Deng, W.; Liu, H. T. DNA-Based Nanofabrication: Pathway to Applications in Surface Engineering. *Small* **2019**, *15*, 1805428.
(25) Surwade, S. P.; Zhao, S. C.; Liu, H. T. Molecular Lithography through DNA-Mediated Etching and Masking of SiO_2. *J. Am. Chem. Soc.* **2011**, *133*, 11868−11871.
(26) Surwade, S. P.; Zhou, F.; Wei, B.; Sun, W.; Powell, A.; O'Donnell, C.; Yin, P.; Liu, H. T. Nanoscale Growth and Patterning of Inorganic Oxides Using DNA Nanostructure Templates. *J. Am. Chem. Soc.* **2013**, *135*, 6778−6781.
(27) Kan, Y. J.; Tan, Q. Y.; Wu, G. S.; Si, W.; Chen, Y. F. Study of DNA Adsorption on Mica Surfaces Using a Surface Force Apparatus. *Sci. Rep.* **2015**, *5*, 8442.
(28) Ricardo, K. B.; Xu, A. Q.; Salim, M.; Zhou, F.; Liu, H. T. Deposition of DNA Nanostructures on Highly Oriented Pyrolytic Graphite. *Langmuir* **2017**, *33*, 3991−3997.
(29) Jin, Z.; Sun, W.; Ke, Y.; Shih, C.-J.; Paulus, G. L.C.; Hua Wang, Q.; Mu, B.; Yin, P.; Strano, M. S. Metallized DNA Nanolithography for Encoding and Transferring Spatial Information for Graphene Patterning. *Nat. Commun.* **2013**, *4*, 1663.
(30) Rothemund, P. W. K. Folding DNA to Create Nanoscale Shapes and Patterns. *Nature* **2006**, *440*, 297−302.
(31) Puri, P.; Yang, V. Effect of Particle Size on Melting of Aluminum at Nano Scales. *J. Phys. Chem. C* **2007**, *111*, 11776−11783.
(32) Yu, Y. H.; Li, Z. D.; Wang, Y. M.; Gong, S. Q.; Wang, X. D. Sequential Infiltration Synthesis of Doped Polymer Films with Tunable Electrical Properties for Efficient Triboelectric Nanogenerator Development. *Adv. Mater.* **2015**, *27*, 4938−4944.
(33) Ediger, M. D.; Forrest, J. A. Dynamics near Free Surfaces and the Glass Transition in Thin Polymer Films: A View to the Future. *Macromolecules* **2014**, *47*, 471−478.
(34) Leng, C. Z.; Losego, M. D. Vapor Phase Infiltration (VPI) for Transforming Polymers into Organic-Inorganic Hybrid Materials: A Critical Review of Current Progress and Future Challenges. *Mater. Horiz.* **2017**, *4*, 747−771.
(35) Bar, G.; Thomann, Y.; Brandsch, R.; Cantow, H. J.; Whangbo, M. H. Factors Affecting the Height and Phase Images in Tapping Mode Atomic Force Microscopy. Study of Phase-Separated Polymer Blends of Poly(ethene-Co-Styrene) and Poly(2,6-Dimethyl-1,4-Phenylene Oxide). *Langmuir* **1997**, *13*, 3807−3812.
(36) Grillo, F.; Van Bui, H.; Moulijn, J. A.; Kreutzer, M. T.; van Ommen, J. R. Understanding and Controlling the Aggregative Growth of Platinum Nanoparticles in Atomic Layer Deposition: An Avenue to Size Selection. *J. Phys. Chem. Lett.* **2017**, *8*, 975−983.
(37) Vervuurt, R. H. J.; Kessels, W. M. M. E.; Bol, A. A. Atomic Layer Deposition for Graphene Device Integration. *Adv. Mater. Interfaces* **2017**, *4*, 1700232.
(38) Liu, W. Y.; Li, L.; Yang, S.; Gao, J.; Wang, R. S. Self-Assembly of Heterogeneously Shaped Nanoparticles into Plasmonic Metamolecules on DNA Origami. *Chem. - Eur. J.* **2017**, *23*, 14177−14181.
(39) Mampallil, D.; Eral, H. B. A Review on Suppression and Utilization of the Coffee-Ring Effect. *Adv. Colloid Interface Sci.* **2018**, *252*, 38−54.

https://dx.doi.org/10.1021/acsnano.0c04493
ACS Nano 2020, 14, 13047−13055